TITLE:

Terahertz spectroscopy of the reactive and radiative near-field zones of split ring resonator

AUTHOR(S):

Blanchard, F.; Ooi, K.; Tanaka, T.; Doi, A.; Tanaka, K.

CITATION:

Blanchard, F. ...[et al]. Terahertz spectroscopy of the reactive and radiative near-field zones of split ring resonator. Optics Express 2012, 20(17): 19395-19403

ISSUE DATE:

2012-08-09

URL:

http://hdl.handle.net/2433/160051

RIGHT:

©2012 Optical Society of America; This paper was published in "Optics Express" and is made available as an electronic reprint with the permission of OSA. The paper can be found at the following URL on the OSA website: http://dx.doi.org/10.1364/OE.20.019395. Systematic or multiple reproduction or distribution to multiple locations via electronic or other means is prohibited and is subject to penalties under law.

京都大学学術情報リポジトリ
KURENAI
Kyoto University Research Information Repository

京都大学 KYOTO UNIVERSITY
A Self-archived copy in
Kyoto University Research Information Repository
https://repository.kulib.kyoto-u.ac.jp
京都大学学術情報リポジトリ KURENAI 紅 Kyoto University Research Information Repository

Terahertz spectroscopy of the reactive and radiative near-field zones of split ring resonator

F. Blanchard,[1,2,*] K. Ooi,[1] T. Tanaka,[1,2] A. Doi,[3] and K. Tanaka[1,2,4]

[1]*Institute for Integrated Cell-Material Sciences (WPI-iCeMS), Kyoto University, Sakyo-ku, Kyoto 606-8501, Japan*
[2]*CREST, Japan Science and Technology Agency, Kawaguchi, Saitama 332-0012, Japan*
[3]*Olympus Corporation 2-3 Kuboyama-cho, Hachioji-shi, Tokyo 192-8512, Japan*
[4]*Department of Physics Graduate School of Science, Kyoto University, Sakyo-ku, Kyoto 606-8502, Japan*
[*]*fblanchard@icems.kyoto-u.ac.jp*

Abstract: A terahertz microscope has been used to excite and observe the resonant modes of a single split ring resonator in the reactive and radiative near-field zones. The two lowest resonant modes of an isolated split ring resonator with their corresponding radiation patterns are reported; they showed good agreement to simulations. The passage from the reactive to radiative near-field zone is also discussed. Further, our result introduced a novel technique to perform terahertz time-domain spectroscopy of samples a few tens of micrometers in size by measuring the in-plane radiative near-field zone.

©2012 Optical Society of America

OCIS codes: (300.6495) Spectroscopy, terahertz; (180.4243) Near-field microscopy; (160.3918) Metamaterials.

References and links

1. D. R. Smith, J. B. Pendry, and M. C. K. Wiltshire, "Metamaterials and negative refractive index," Science **305**(5685), 788–792 (2004).
2. J. B. Pendry, "Negative refraction makes a perfect lens," Phys. Rev. Lett. **85**(18), 3966–3969 (2000).
3. D. Schurig, J. J. Mock, B. J. Justice, S. A. Cummer, J. B. Pendry, A. F. Starr, and D. R. Smith, "Metamaterial electromagnetic cloak at microwave frequencies," Science **314**(5801), 977–980 (2006).
4. J. B. Pendry, A. Holden, D. Robbins, and W. Stewart, "Magnetism from conductors and enhanced nonlinear phenomena," IEEE Trans. Microw. Theory Tech. **47**(11), 2075–2084 (1999).
5. J. Zhou, T. Koschny, and C. M. Soukoulis, "Magnetic and electric excitations in split ring resonators," Opt. Express **15**(26), 17881–17890 (2007).
6. R. R. A. Syms, E. Shamonina, V. Kalinin, and L. Solymar, "A theory of metamaterials based on periodically loaded transmission lines: Interaction between magnetoinductive and electromagnetic waves," J. Appl. Phys. **97**(6), 064909 (2005).
7. V. G. Veselago, "Waves in metamaterials: their role in modern physics," Phys.-Usp. **54**(11), 1161–1165 (2011).
8. M. L. Povinelli, S. G. Johnson, J. D. Joannopoulos, and J. B. Pendry, "Toward photonic-crystal metamaterials: Creating magnetic emitters in photonic crystals," Appl. Phys. Lett. **82**(7), 1069–1071 (2003).
9. D. Grischkowsky, S. Keiding, M. van Exter, and C. Fattinger, "Far-infrared time-domain spectroscopy with terahertz beams of dielectrics and semiconductors," J. Opt. Soc. Am. B **7**(10), 2006–2015 (1990).
10. A. K. Azad, J. Dai, and W. Zhang, "Transmission properties of terahertz pulses through subwavelength double split-ring resonators," Opt. Lett. **31**(5), 634–636 (2006).
11. H. Tao, W. J. Padilla, X. Zhang, and R. D. Averitt, "Recent progress in electromagnetic material devices for terahertz applications," IEEE J. Sel. Top. Quantum Electron. **17**(1), 92–101 (2011).
12. A. J. L. Adam, "Review of near-field terahertz measurement methods and their applications," J. Infrared Millimeter Waves **32**(8-9), 976–1019 (2011).
13. G. Acuna, S. F. Heucke, F. Kuchler, H.-T. Chen, A. J. Taylor, and R. Kersting, "Surface plasmons in terahertz metamaterials," Opt. Express **16**(23), 18745–18751 (2008).
14. A. Bitzer, H. Merbold, A. Thoman, T. Feurer, H. Helm, and M. Walther, "Terahertz near-field imaging of electric and magnetic resonances of a planar metamaterial," Opt. Express **17**(5), 3826–3834 (2009).
15. J. Wallauer, A. Bitzer, S. Waselikowski, and M. Walther, "Near-field signature of electromagnetic coupling in metamaterial arrays: a terahertz microscopy study," Opt. Express **19**(18), 17283–17292 (2011).
16. H. Merbold, A. Bitzer, F. Enderli, and T. Feurer, "Spatiotemporal visualization of THz near-fields in metamaterial Arrays," J. Infrared, Millimeter Terahertz Waves **32**(5), 570–579 (2011).
17. "IEEE standards definitions of terms for antennas," IEEE Std 145–1993, 10.1109/IEEESTD.1993.119664 (1993).

#169662 - $15.00 USD Received 1 Jun 2012; revised 26 Jul 2012; accepted 27 Jul 2012; published 9 Aug 2012
(C) 2012 OSA

京都大学 KYOTO UNIVERSITY
A Self-archived copy in
Kyoto University Research Information Repository
https://repository.kulib.kyoto-u.ac.jp
京都大学学術情報リポジトリ KURENAI 紅 Kyoto University Research Information Repository

18. S. Laybros, P. F. Combes, and H. J. Mametsa, "The "very-near-field" region of equiphase radiating apertures," IEEE Ant. Prop. Mag. **47**(4), 50–66 (2005).
19. F. Blanchard, A. Doi, T. Tanaka, H. Hirori, H. Tanaka, Y. Kadoya, and K. Tanaka, "Real-time terahertz near-field microscope," Opt. Express **19**(9), 8277–8284 (2011).
20. A. Doi, F. Blanchard, T. Tanaka, and K. Tanaka, "Improving spatial resolution of real-time terahertz near-field microscope," J. Infrared, Millimeter, Terahertz Waves **32**(8-9), 1043–1051 (2011).
21. H. Hirori, A. Doi, F. Blanchard, and K. Tanaka, "Single-cycle terahertz pulses with amplitudes exceeding 1 MV/cm generated by optical rectification in $LiNbO_3$," Appl. Phys. Lett. **98**(9), 091106 (2011).
22. E. D. Palik, *Handbook of Optical constants of solids* (Academic Press handbook series, 1985).
23. M. A. Seo, H. R. Park, S. M. Koo, D. J. Park, J. H. Kang, O. K. Suwal, S. S. Choi, P. C. M. Planken, G. S. Park, N. K. Park, Q. H. Park, and D. S. Kim, "Terahertz field enhancement by metallic nano slit operating beyond the skin-depth limit," Nat. Photonics **3**(3), 152–156 (2009).
24. M. A. bin A. Wahab, A. H. Awang and R. S. S. A. Kadir, "An investigation of square split-ring resonator as antenna operating at terahertz frequency," Asia-Pacific Conference on Appl. Elec. proceeding (2007).
25. M. Skorobogatiy and J. Yand, *Photonic Crystal Guiding* (Cambridge University Press, 2009).
26. C. Rockstuhl, F. Lederer, C. Etrich, T. Zentgraf, J. Kuhl, and H. Giessen, "On the reinterpretation of resonances in split-ring-resonators at normal incidence," Opt. Express **14**(19), 8827–8836 (2006).
27. L. Novotny and B. Hecht, *Principles of Nano-Optics* (Cambridge university press, 2006), chap. 8.

1. Introduction

Over the past few years, metamaterials have attracted much attention due to their unique ability to be engineered to obtain desired electromagnetic (EM) properties at optical wavelengths [1]. These artificial structured materials have demonstrated such exotic properties as negative refractive index, perfect lensing, and cloaking [1–3]. The most common metamaterial is an array of split ring resonators (SRR), where the unit cell is smaller than the wavelength and consists of a metallic ring separated in one point by a gap [4]. In many cases, the optical response of an SRR is analyzed in analogy to a simple *LC* resonator [5], and coupling between SRRs is recognized as mutual inductance [6]. However, the asymmetric nature of SRR leads to non-uniform EM field radiation in the Fresnel zone (or radiative near-field zone) that must be known in order to design efficient metamaterials. For instance, SRRs must be positioned at specific intervals to optimize the different characteristics of the metamaterials [7,8]. Most prominent applications involve the propagation of magneto-inductive waves inside metamaterials [7] achieved through near-field interactions between SRRs ($\lambda > d$), and metamaterials with $\lambda < d$ geometry that exhibits behaviors of photonic crystals [8], where d is the lattice parameter and λ is the wavelength. Ideally for both cases, phase information contained in the surrounding field of each unit cell must match its neighbors.

Several reports using terahertz (THz) radiation have demonstrated the great potential of THz time-domain spectroscopy (THz-TDS) techniques [9] to study the amplitude, phase and polarization dependence of metamaterials [10,11]. More recently, near-field THz imaging techniques [12] have proven to be a powerful tool to characterize the complex behavior of metamaterials in a subwavelength scale [13–16]. The electric and magnetic resonances of a planar metamaterial have been directly mapped [13,14], and the coupling between elements in SRR arrays have been studied [13,15]. The visualization of the spatiotemporal evolution of a THz pulse transmitted through and reflected from SRR arrays [16] has also been demonstrated. To the best of our knowledge, no work has been done in describing the in-plane EM fields in the reactive and radiative near-field zones from an isolated SRR. This additional information may significantly help to clarify the EM field distribution and phase of THz waves in regions close to the sample (i.e., from $\lambda > d$ *to* $\lambda < d$).

In this work, we visualized two resonant modes of an isolated SRR by electro-optic (EO) detection of the sample reactive and radiative near-field zones [17,18] using a large field-of-view THz microscope. The near-field information obtained locally inside a single SRR agreed well with the information contained in the in-plane radiated near-field THz waves, which was also confirmed by simulations carried out using finite domain time difference (FDTD) software (Lumerical). In the frequency domain, the near-field maps revealed the singularity of

#169662 - $15.00 USD Received 1 Jun 2012; revised 26 Jul 2012; accepted 27 Jul 2012; published 9 Aug 2012
(C) 2012 OSA

京都大学 KYOTO UNIVERSITY
A Self-archived copy in
Kyoto University Research Information Repository
https://repository.kulib.kyoto-u.ac.jp
京都大学学術情報リポジトリ KURENAI 紅 Kyoto University Research Information Repository

the radiation patterns of SRR for the two lowest resonances while time-domain information clarified the passage from reactive to radiative near-field zones.

2. Experimental

To perform our experiment, we used a real-time THz microscope, as previously reported [19]. In this microscope system, a large probe beam at 800 nm illuminated a thin $LiNbO_3$ (LN) crystal used for 2-dimensional electro-optic (EO) imaging in reflection scheme. The SRR samples were fabricated by standard photolithography of a 100-nm-thick gold layer on the high reflecting coating side of a 3-μm-thick *x*-cut $LiNbO_3$ (LN) wafer mounted on a 500-μm-thick glass substrate (*Tempax* from Schott). We selected a 3-μm-thick electro optic (EO) crystal to improve the spatial resolution to 10 μm [20]. The losses in sensitivity caused by a thin EO crystal were compensated by a tightly focused THz pulse with peak electric field of >600 kV/cm ranging from 0.1 to 2.5 THz [21]. Notice that the high reflective (HR) coating side for the probe beam (SiO_2 made) has the same thickness as the LN crystal.

To evaluate the resonant modes of SRR, we characterized three samples consisting of square SRRs with different sizes (Fig. 1(a)). Gap size d and width w were kept constant for each sample and only length l was varied. The SRR dimensions are d = 4 μm, w = 9 μm, and l = 50 μm, 60 μm and 70 μm for SRRs (1), (2) and (3), respectively. We present in Figs. 1(a) and 1(b) a visible and schematic description of the samples. The THz excitation polarization and the probe beam (λ_{800nm}) polarization were set parallel to each other following the gap orientation. To maximize the EO signal, all SRR were patterned with their gap oriented 45° with respect to the crystal axis, i.e., relative to n_O and n_{EO} (Fig. 1(a)). The radiated THz waves were measured for the same polarization direction as the exciting beam and parallel to the gap (Fig. 1(b)). For convenience, we define *x*-axis direction following the gap orientation, as illustrated in Fig. 1(b).

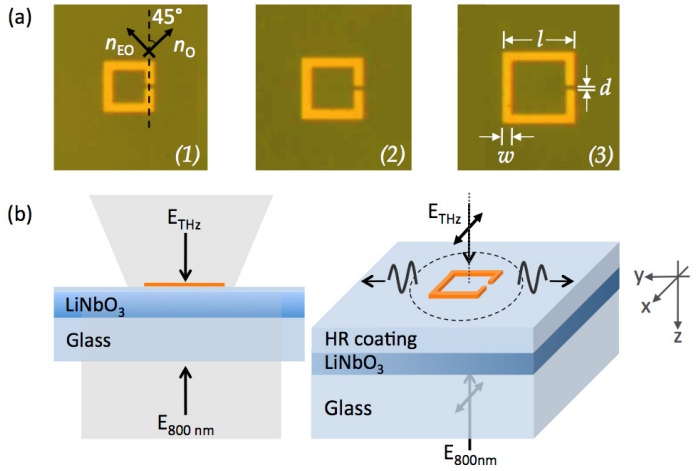

Fig. 1. Visible image of three squares (a) SRRs; the SRR dimensions are d = 4 μm, w = 9 μm, and l = 50 μm, 60 μm and 70 μm for SRRs (1), (2) and (3), respectively; (b) schematic of the excitation and detection of radiated THz waves.

Under our experimental conditions, all field components (E_x, E_y and E_z) are simultaneously excited by the SRR structure. By using an *x*-cut LN crystal as EO sensor and following the axis definition presented in Fig. 1, E_z field measurement is not possible, but crosstalk between E_x and E_y field components remains due to non-zero EO tensors. However, we confirmed by comparing our results with simulations that E_x field (i.e., field parallel to gap orientation) is the dominant component in all our measurements.

#169662 - $15.00 USD Received 1 Jun 2012; revised 26 Jul 2012; accepted 27 Jul 2012; published 9 Aug 2012
(C) 2012 OSA

京都大学 KYOTO UNIVERSITY
A Self-archived copy in
Kyoto University Research Information Repository
https://repository.kulib.kyoto-u.ac.jp
京都大学学術情報リポジトリ KURENAI 紅 Kyoto University Research Information Repository

3. Results

3.1. Resonances in time-domain

Figure 2 shows the THz electric field evolution in the near-field region of a gold SRR after irradiation of a THz excitation pulse. A movie obtained without a sample served as a reference. Both movies (sample and reference) are 500 frames long with a 27-fs time step. (We note here that the frequency-domain analysis was restricted by our 500-μm-thick glass substrate that returned an echo 7.12 ps after the main peak. The frequency resolution of our sensor can probably be improved with a thicker substrate with less absorptive material). We subtracted the reference movie from the sample movie in order to clarify the resonant modes and diffracted field propagating for x and y directions. After this operation and because the exciting beam is propagating in the z direction, only the x and y oriented **k**-vector fields remain around the sample. Figure 2(a) is a schematic view of the sample, and a snapshot sequence (from (b) to (f)) is shown for sample (1), where l = 50 μm. Within this snapshot series, the lowest resonant mode can be observed inside the SRR with a re-emitted higher frequency around the sample. Notice that the selected snapshots (d), (e), and (f) reveal one oscillating period of the lowest resonant mode inside the sample.

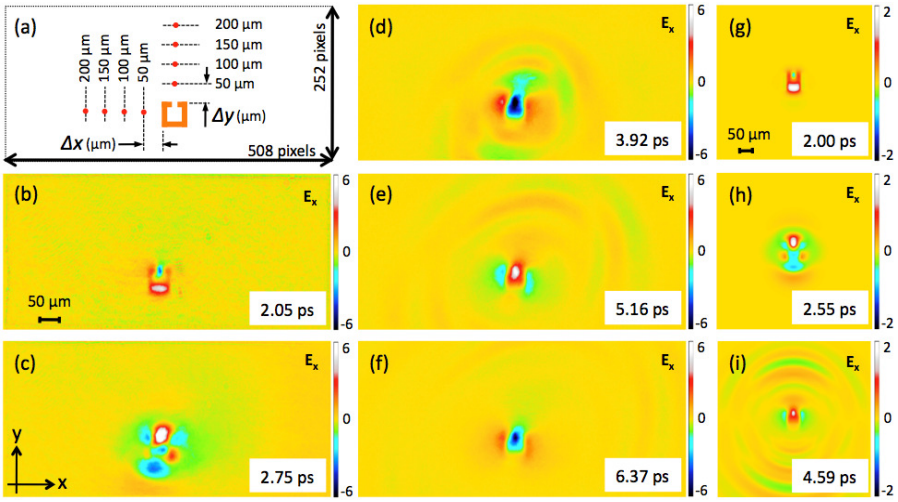

Fig. 2. (a) Sketch illustrating measurement positions of laterally radiated E_x fields; (b) to (f) series of snapshots obtained for sample (1); (g) to (i) series of snapshots simulated for sample (1). Experimental (Media 1) and simulated (Media 2) movies are available online. The image distortion observed in the experiment is attributed to birefringence of LN crystal [19].

We validated our measurements using FDTD software that reproduced the experimental conditions. The simulations were performed using a Gaussian THz excitation beam shape ranging from 0.1 to 2.5 THz in bandwidth with polarization set parallel to the gap. A 0.4 x 0.4 x 1 mm^3 size substrate and a 0.4 x 0.4 mm^2 by 3-μm-thick high reflective coating material were set using the optical constants of SiO_2 [22]. The thicker substrate was selected to extend the simulation range to 15 ps without disturbance of a second echo. A 3-μm-thick x-cut LN crystal with a refractive index of 5.8 was inserted between the two glass layers. Since we patterned the SRRs with an angle onto the LN crystal, the agreement between experiments and simulations was found by tuning the average refractive index value of LN material. All SRR structures were simulated using the dielectric parameters of gold [23]. For each sample, we simulated the E_x, E_y, and E_z components of the electric field with an additional movie without a sample, which was used as reference data. Figure 2(g) to 2(i) is a snapshot sequence of the simulated fields for sample (1), which also exhibits the expansion THz field around the sample.

#169662 - $15.00 USD Received 1 Jun 2012; revised 26 Jul 2012; accepted 27 Jul 2012; published 9 Aug 2012
(C) 2012 OSA

京都大学 KYOTO UNIVERSITY
A Self-archived copy in
Kyoto University Research Information Repository
https://repository.kulib.kyoto-u.ac.jp
京都大学学術情報リポジトリ KURENAI 紅 Kyoto University Research Information Repository

Figure 3(a) shows the measured THz pulse waveforms obtained at the gap position of the three samples with the reference pulse used for sample (1). The corresponding Fourier transforms normalized to their respective references are shown in Fig. 3(b). Zero padding technique was used for all Fourier transforms data, which produces a longer FFT vector and results in a smoother looking spectrum. Three distinct resonances appear in the spectra for 0.45, 0.37 and 0.32 THz that relate to the different sized square SRRs from the smallest (1) to the largest (3). We found that these resonant modes scaled linearly with the geometric factor $1/l$ of our SRRs, as previously predicted [24]. Notice that only one resonant mode could be observed at the gap position of each sample. Using the data presented in Fig. 3(a) and 3(b), we also evaluated the field enhancement factor at the SRR's gap position. A measured enhancement factor of 4.2 is found experimentally, which corresponds to a real enhancement factor of 40 [19] (i.e., between the gap at the crystal surface position). The difference is mainly due to a measured enhancement factor that rapidly decreased as the detection location gets farther from the gap position [19]. Portions (c) and (d) of Fig. 3 are the simulated data corresponding to the experimental results presented in (a) and (b). We found higher enhancement factor with a higher Q-factors for the simulation case. We explain this small deviation from the more absorptive substrate with a higher refractive index used in our experiment when compared to SiO_2 material used in simulation. Nonetheless, the simulations remain in good agreement with our measurements and should therefore be used to analyze our experimental results.

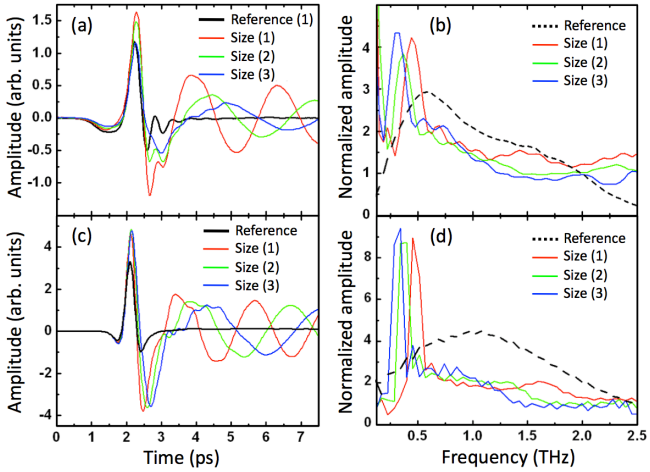

Fig. 3. Measured resonant fields at gap positions: (a) our samples with reference THz pulse excitation; (b) normalized Fourier transforms of THz pulses presented in (a); Figs. (c) and (d) are simulated data corresponding to (a) and (b).

3.2. Resonances by radiated field

Following the good calibration results obtained with our simulation tool, we studied the THz waves that were radiated around the sample and that propagated laterally when compared to the exciting THz pulse. We extracted the time-domain information at several positions from the SRR gap. Figures 4(a) to 4(d) show the Fourier transformed spectra of the experimental and simulated radiated THz fields normalized to the reference pulse for sample (1). The pulses are measured for different Δx or Δy positions on the EO crystal (red dots in Fig. 2(a)), varying from a distance of 50 to 200 μm of the gap position. Using the radiated beam in the y direction, we found a first resonant mode at 0.40 THz (Fig. 4(a)) that corresponds to the resonant mode presented in Fig. 3(b). In addition to the first resonant mode, a higher and broader resonant mode is identified at 1.66 THz for the y direction in sample (1). This resonance almost vanishes for x direction simulations whereas it dropped below noise level

#169662 - $15.00 USD Received 1 Jun 2012; revised 26 Jul 2012; accepted 27 Jul 2012; published 9 Aug 2012
(C) 2012 OSA

京都大学 KYOTO UNIVERSITY
A Self-archived copy in
Kyoto University Research Information Repository
https://repository.kulib.kyoto-u.ac.jp
京都大学学術情報リポジトリ KURENAI 紅 Kyoto University Research Information Repository

for measurements (Fig. 4(b)), and this strongly suggests a different emission pattern for both resonant modes.

One clear visual distinction between the two resonant modes observed in time-domain data (Figs. 2(b) to 2(f)) is the larger size of the expansion field around the sample coming from the higher resonant mode. Since such energy rapidly radiated (i.e., indicating large radiative losses) outside the SRR, a weakly confined resonance and broader linewidth of the mode at 1.66 THz are expected, as observed in Fig. 4(a). Finally, the experimental data for the *x* and *y* directions are in good agreement with the simulations (Figs. 4(c) and 4(d)), which confirmed the ability to retrieve the THz signature of a sample by measuring the THz waves in the radiative near-field region.

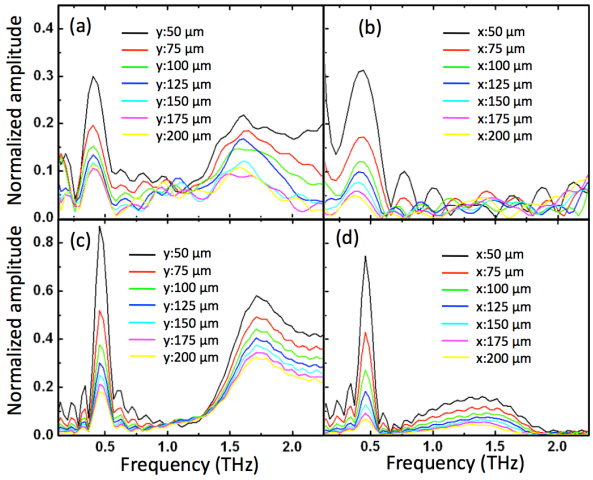

Fig. 4. Measured Fourier spectra of time-domain spectroscopy of the radiated field for Δy positions (a) and Δx positions (b) on the EO crystal. Simulated Fourier spectra of time-domain spectroscopy of the radiated field for Δy positions (c) and Δx positions (d) on the EO crystal.

3.3. Resonances in frequency domain

To clarify the origin of the resonant modes, we show in Fig. 5 the Fourier transforms of near-field maps for the two lowest resonant modes obtained for our experimental and simulated data done on sample (1). More precisely, Fig. 5(a) is obtained by Fourier transforming the measured temporal evolution of the E_x scattered field, partly shown in Figs. 2(b) to 2(f), and Figs. 5(b) to 5(d) show the simulated E_x, E_y, and E_z field components, respectively. Notice that simulated field distributions were calculated 5 μm below the surface of the crystal, which accurately represents the experimental conditions [19]. The good agreement found between the measured and simulated E_x fields in Figs. 5(a) and 5(b) imply a trustworthy interpretation of the calculated E_y and E_z components since FDTD calculations obtained all EM fields simultaneously. In Fig. 5, we see that both resonant modes have symmetric E_x and antisymmetric E_y and E_z components in respect to the $x = 0$ plane. These symmetric and antisymmetric electric field distributions are attributed to the symmetry of the SRR in addition to the symmetry of the incident electric field. Since the SRR has mirror symmetry at the $x = 0$ plane (i.e., $\varepsilon(x,y,z) = \varepsilon(-x,y,z)$ and $\mu(x,y,z) = \mu(-x,y,z)$), the resonant modes must have the electromagnetic field distributions of one of two prescribed symmetries [25].

Next, we qualitatively discuss the charge and current distributions on the SRR when the two resonant modes shown in Fig. 5 are excited. For this, we consider the SRR in a homogeneous, linear, and isotropic space. Under this simplification, the radiated electric field can be divided into two parts. One originates from the surface current on the SRR, and the other originates from the surface charges accumulated by the non-uniform distribution of the surface current. Under the assumption that gold is a perfect conductor at THz frequencies, the

#169662 - $15.00 USD Received 1 Jun 2012; revised 26 Jul 2012; accepted 27 Jul 2012; published 9 Aug 2012
(C) 2012 OSA

京都大学 KYOTO UNIVERSITY
A Self-archived copy in
Kyoto University Research Information Repository
https://repository.kulib.kyoto-u.ac.jp
京都大学学術情報リポジトリ KURENAI 紅 Kyoto University Research Information Repository

field normal to the metallic surface directly reflects the charge distribution. From the upper figure of Fig. 5(d), we can see that charges are accumulated at both ends of the gap position, which indicates *LC* type resonance (i.e., current flow from one end of the gap side to the other). From the lower figure of Fig. 5(d), we can see that the second lowest mode at 1.66 THz forms a quadrupole, which agrees with THz [12,15] and near-infrared studies [5,26] done on SRRs. Notice that in Fig. 5(b) and 5(c), E_y field is 3 times weaker than E_x field, which help to reduce crosstalk when using a 3-μm-thick *x*-cut LN EO sensor.

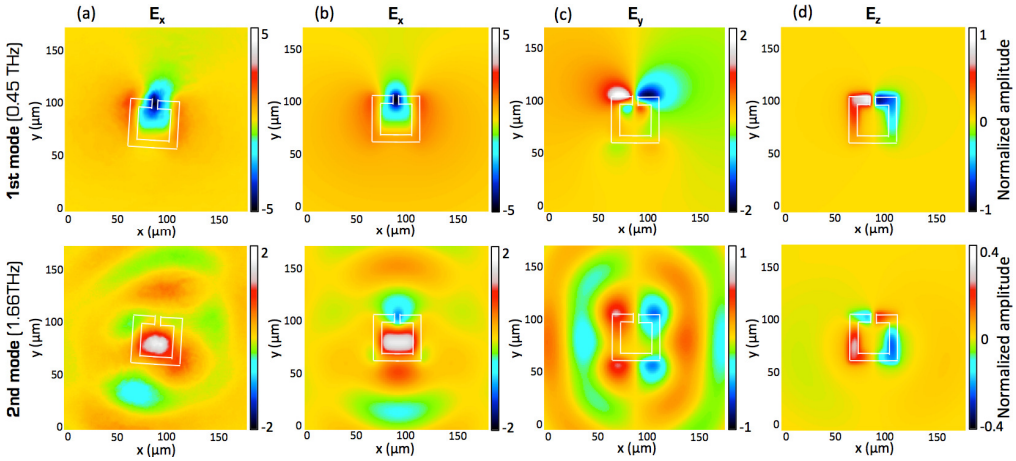

Fig. 5. Real part of measured E_x (a) and simulated E_x (b), E_y (c), and E_z (d) electric field distributions for first two resonant modes. The THz field excitation polarization was kept parallel to the gap for all data.

3.4. Resonances in the reactive and radiative near-field zones

As mentioned earlier, the lowest mode of the SRR is the *LC* type resonance since the current flows from one end of the gap to the other. This means the electric field of the lowest mode is created from both the accumulated charge at the gap position, and current, which flows along the SRR. However, we can see from the upper figure of Fig. 5 that the electric field is concentrated only at the gap position. This implies that the electric field generated from the charge distribution is dominant compared with that generated from current very close to the source (for $\lambda >> |\mathbf{x}\text{-}\mathbf{x}'|$, with **x** and **x**' the positions of the dipole and observation point, respectively) [27].

We tested this condition for THz waveforms traveling in the *y* direction from the gap position (red dots in Fig. 2(a)) and found two distinctive zones, shown in Fig. 6. We noticed that charge emission behavior mainly occurred in a region very close to the gap ($y < 75$ μm), where the field amplitude decays at $>1/r^2$, and the phase remains constant. A second zone appears for $y > 75$ μm where the *LC*-resonance field transited to a $>1/r$ amplitude dependence and slowly experienced a phase shift for distances larger than 50 μm from the gap position; this clearly indicates radiative behavior. These decaying behaviors are in good agreement with a previously reported near-field and intermediated field description [27]. For a very short dipole, or an equivalent radiator, we can define the outer boundary of the reactive near-field zone to exist at a distance $\lambda/2\pi$ from the radiator surface [18]. By assuming plasmonic resonances [26] in the SRR, we can approximate the wavelength of the lowest mode by $\lambda/2$ of the SRR size length, which corresponds to 400 μm for sample (1). Thus, the reactive near-field boundary is estimated to be 64 μm according to [18], which corresponds to the zone with constant phase in our experiment.

#169662 - $15.00 USD Received 1 Jun 2012; revised 26 Jul 2012; accepted 27 Jul 2012; published 9 Aug 2012
(C) 2012 OSA

京都大学 KYOTO UNIVERSITY
A Self-archived copy in
Kyoto University Research Information Repository
https://repository.kulib.kyoto-u.ac.jp
京都大学学術情報リポジトリ KURENAI 紅 Kyoto University Research Information Repository

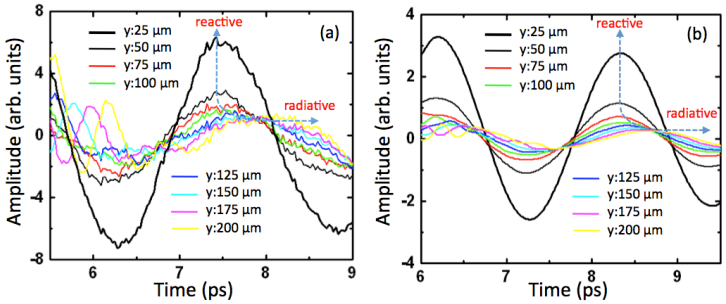

Fig. 6. (a) Experimental and (b) simulated THz pulses laterally propagating in *y* direction when compared to the exciting THz pulse.

Finally, to visualize the reactive and radiative near-field zones simultaneously, we adopted a representation on a logarithmic scale normalized to the Fourier components of the THz field without a sample. In Fig. 7, we show the measured (a) $|E_x|$ and simulated (b) $|E_x|$, (c) $|E_y|$, and (d) $|E_z|$ radiation patterns plotted in dB for a single SRR. These results are evidence of the different radiation patterns for the two lowest resonant modes of the SRR. For the $|E_x|$ component, *LC*-resonance generates a three-lobe emission pattern, whereas quadrupole resonance leads to higher emission directivity in the *y* direction with complete suppression of radiated energy in the *x* direction. In Media 3 and Media 4, we present the measured and simulated radiation patterns in dB for $|E_x|$ ranging from 0.1 to 2.5 THz. As visualized in these two movies, the radiation patterns have different frequency dependences for positive and negative *y*-directions of the SRR (i.e., for gap side and opposite side). This may be due to the asymmetric geometry of the upper and lower parts of the SRR, which suppressed, or built up, certain radiated frequencies in a preferential direction and may also explain why the second lowest mode is very broad.

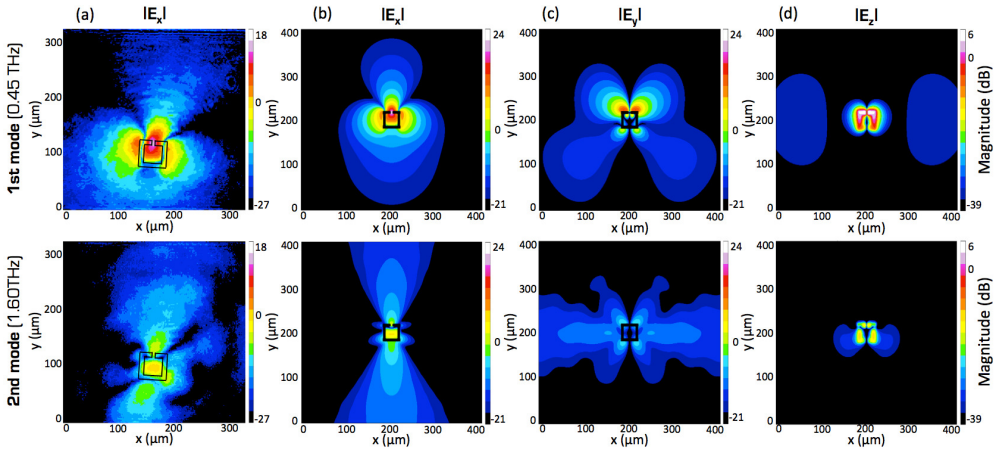

Fig. 7. Magnitude of (a) measured (a) (Media 3) and (b) simulated (b) (Media 4) electric field distributions for two first two resonant modes for $|E_x|$;, simulated electric field distribution for (c) $|E_y|$ (c) and (d) $|E_z|$ field components (c).

4. Conclusion

In conclusion, we successfully identified the two lowest resonance modes of an SRR with their associated radiation patterns. Our results agree well with simulations and previous studies done at THz frequency and in the near infrared range. In addition, by combining the near-field THz maps with time-domain spectroscopy, we clarified the passage from reactive to radiative near-field zones of the SRR at 0.45 THz. Knowing the field evolution around an isolated SRR may have a significant impact on the design of efficient metamaterials due to

#169662 - $15.00 USD Received 1 Jun 2012; revised 26 Jul 2012; accepted 27 Jul 2012; published 9 Aug 2012
(C) 2012 OSA

京都大学 KYOTO UNIVERSITY
A Self-archived copy in
Kyoto University Research Information Repository
https://repository.kulib.kyoto-u.ac.jp
京都大学学術情報リポジトリ KURENAI 紅 Kyoto University Research Information Repository

the phase information contained in the surrounding field of each unit cell that must match its neighbors. Further, we reported an alternative way of performing THz time-domain spectroscopy of subwavelength-size samples using radiated THz waves that propagate laterally inside the electro-optic crystal when compared to a THz excitation beam.

Acknowledgments

The iCeMS is supported by World Premier International Research Center Initiative (WPI), MEXT, Japan. We wish to acknowledge financial support from MEXT/JSPS KAKENHI grants number 23244065 and 00571358. F. B. wishes to acknowledge Le Fonds Québécois de la Recherche sur la Nature et les Technologies (FQRNT) contract number 138131.

#169662 - $15.00 USD Received 1 Jun 2012; revised 26 Jul 2012; accepted 27 Jul 2012; published 9 Aug 2012
(C) 2012 OSA